Time-Resolved Infrared Spectroscopy of Molecular Reorientation During FLC Electro-Optic Switching

Won Gun Jang
Korea Photonics Technology Institute (KOPTI) 459-3 Bonchon-dong, Buk-gu, Gwangju 500-210, KOREA

Noel A. Clark
Ferroelectric Liquid Crystals Materials Research Center (FLCMRC), Department of Physics, University of Colorado at Boulder, CO 80309 USA.

Abstract

*Polarized Fourier transform infrared (IR) absorption is used to probe molecular conformation in a ferroelectric liquid crystal (FLC) during the reorientation induced by the external field. Spectra of planar aligned cells of FLC **W314** are measured as functions of IR polarizer orientation and electric field applied to the FLC. The time evolution of the dichroism of the absorbance due to biphenyl core and alkyl tail molecular vibration modes, is observed. Static IR dichroism experiments show a **W314** dichroism structure in which the principal axis of dielectric tensor from molecular core vibration are tilted further from the smectic layer normal than those of the tail. This structure indicates the effective binding site in which the molecules are confined in the Sm-C phase has, on average, "zig-zag" shape and this zig-zag binding site structure is rigidly maintained while the molecular axis rotates about the layer normal during field-induced switching.*

1. Introduction

Infrared (IR) dichroism has proven to be a powerful probe of the molecular conformation and organization in liquid crystal phases. IR spectroscopy selects molecular vibrational modes, each of which has a transition dipole, fixed relative to the molecule, which couples the vibration to incident IR light. Measurement of IR absorbance vs. polarization orientation relative to the symmetry axes of a macroscopically single domain sample then enables the moments of the transition dipole, and, therefore, of the molecular orientation distribution to be determined. It is interesting to apply this technique to the lower symmetry liquid crystal (LC) phases, such as the smectic C (Sm-C) and the ferroelectric liquid crystal (FLC) chiral smectic C (Sm-C*), which is macroscopically polar. Recently Fourier Transform IR (FTIR) studies of FLCs have probed the origin of ferroelectricity via static dichroism measurements [1, 2], and changes in molecular orientation during electric-field-induced switching via time-resolved spectroscopic (TRS) IR dichroism measurements [3,4]. Macroscopic polar ordering in liquid crystals (LC's) was discovered in the chiral smectic C (Sm-C*) liquid crystal **DOBAMBC** by Meyer et al. [5] and has been intensively studied since the demonstration of ferroelectric domains and fast, bistable, electro-optic effects in the bookshelf surface stabilized ferroelectric (SSFLC) cell geometry of Fig. 1 [6]. SmC* liquid crystals are fluid ferroelectrics, characterized by the structure shown in Figure 1, a one dimensional (1D) stacking of 2D liquid layers of rod-shaped molecules having a mean long molecular axis (optic axis) tilted through a fixed angle θ from the layer normal. Such a phase is required by the chiral symmetry to have a macroscopic spontaneous ferroelectric polarization $\mathbf{P}_s$, locally normal to the mean long axis **n** and to the layer normal **z**. Although the magnitude of $\mathbf{P}_s$ is fixed, depending only on temperature, the azimuthal orientation $\phi(\mathbf{r})$ responds to applied electric field, surface interactions, and elasticity of the director field $\mathbf{n}(\mathbf{r})$. For a square-wave voltage of large amplitude applied to the cell geometry of Figure 1 $\mathbf{n}(\mathbf{r})$ is spatially uniform and is driven by the field around on the tilt cone, saturating at $\phi = 0$ for $V > 0$ and at $\phi = \pi$ for $V < 0$. In this work we present TRS measurements of the field-induced fast collective molecular reorientation of an FLC and the relative motion of major molecular sub-fragments (phenyl, nitro core and

alkyl tail). With field applied the Sm-C* tilt plane normal to the incident IR light, so that by varying the IR polarization one can then probe the orientation of the absorption dipoles in the tilt plane.

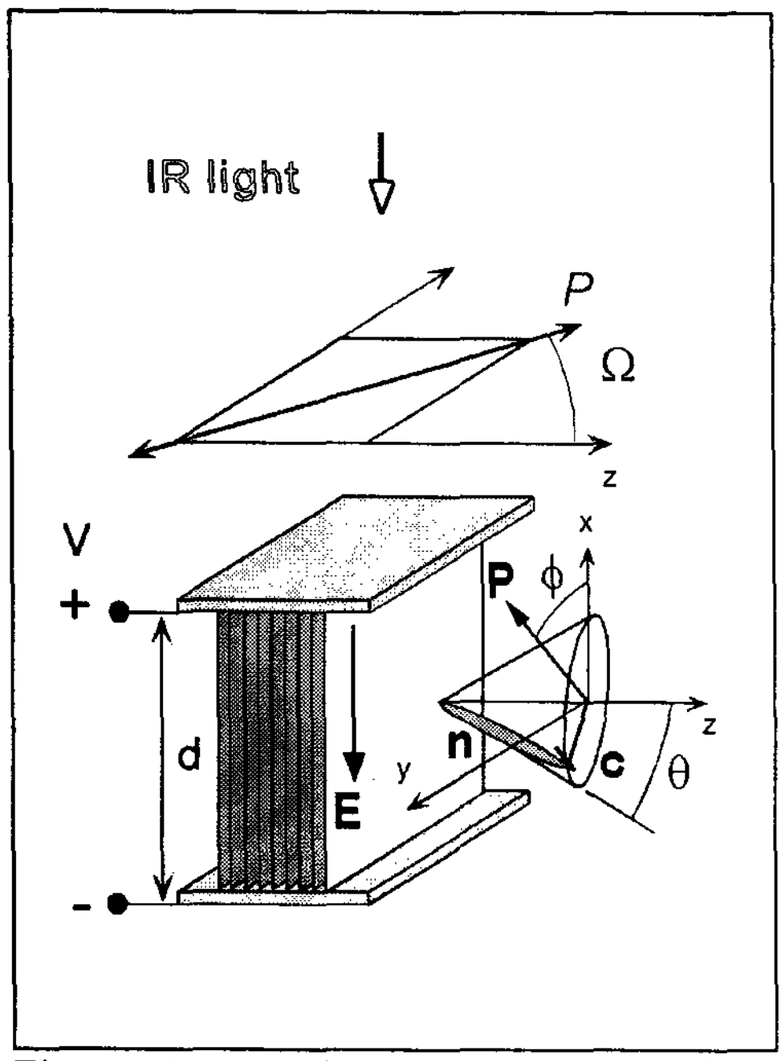

Figure 1. A schematic diagram of the FTIR experiment.

2. Experiment

The experimental cell geometry is represented in Figure 1 and the electronic setup shown in Figure 2. Step-scan FT-IR time-resolved spectroscopy (TRS) is conducted using a Bruker IFS 66 FT-IR spectrometer. A photo-voltaic mercury cadmium telluride (MCT) detector with a 50 MHz preamplifier and an internal ADC board is used to detect the modulated IR signal. A square wave voltage is applied to the liquid crystal cell using a function generator (V_{pp}=12 V), and synchronized TTL trigger pulse signals for data sampling are fed onto the 16-bit analog-to-digital converter of the main spectrometer. Spectrometer transmission is collected while both interferometer path difference and time delay following reversal of the voltage on the FLC cell are changing. 30 independent measurements are made at each mirror position and time delay. The computer then sorts, averages, and Fourier transforms the data to obtain spectra vs. time delay.

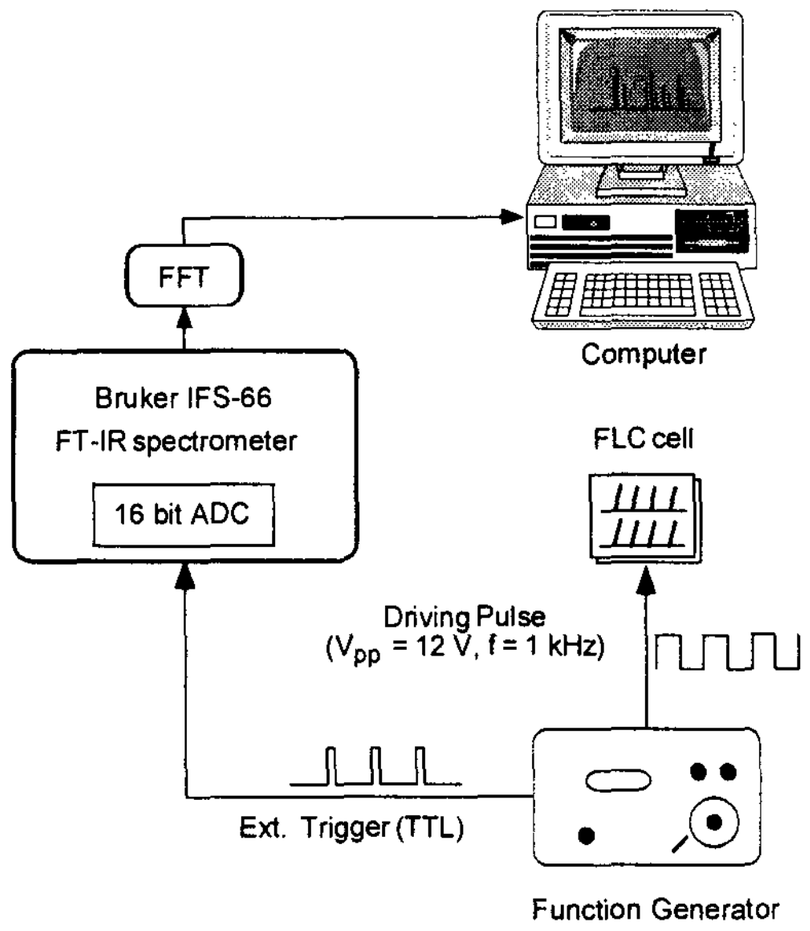

Figure 2. FTIR time-resolved spectroscopy setup. A 1kHz 12 V_{pp} square wave is applied to the FLC cell and synchronized TTL trigger pulse signals for data sampling are fed onto the 16-bit A/D converter of main spectrometer.

Raw spectra are then baseline corrected and values of absorbance peaks determined. Data are presented here for peaks at 2927, 1736, 1606 and 1535 cm^{-1}, due to the *alkyl* tail, *carbonyl* group, *phenyl* core and *nitro* group stretching modes respectively. A wire-grid IR polarizer is positioned between the IR source and sample and its orientation Ω, is set at 10° intervals, with Ω = 0° having IR polarization is parallel to layer normal. Spectra are measured for the full range of time delay for each setting of Ω. Spectra were recorded at 4 cm^{-1} spectral resolution in consecutive time series of 5 μs intervals up to a maximum delay after reversal of 500 μs, limited by the applied frequency of 1 kHz. **W314**, shown in Figure 3 along with its phase diagram. **W314** has negative spontaneous polarization of large magnitude ($0 < |\mathbf{P}_s| < 426$ nC/cm^2), which is mainly due to the electronegative constituent - NO_2.

The electro-optic cells were IR and visible light transparent capacitors made from CaF_2 windows coated with a thin layer of indium-tin oxide (ITO) for electrodes and spaced to a LC thickness of 2 to 3 μm by uniform polymer balls.

The cells were filled with W314 in the Isotropic

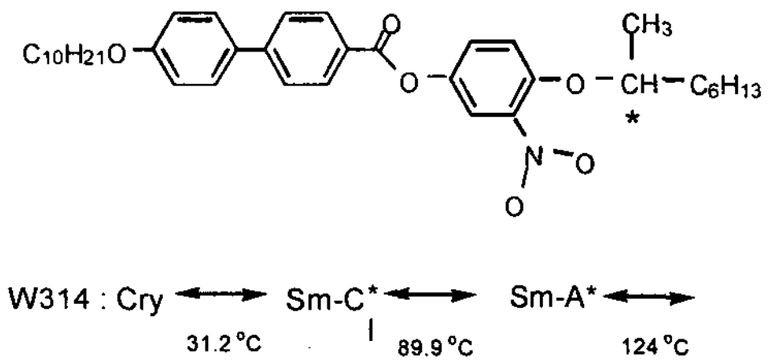

Figure 3. Phase diagram and chemical structure of ferroelectric liquid crystal compound **W314**.

phase and cooled slowly into the SmA* and SmC* phases. The layer structure obtained upon cooling into the SmC* phase was chevron, but the voltage threshold for deforming the chevron structure into the bookshelf was quite low (several volts), so that the IR experiments were always carried out in the bookshelf geometry.

Initial evaluation of a cell and its time response was obtained in the SmC* phase by setting $\Omega \approx \theta$ such that the IR polarization vector is parallel to liquid crystal director, **n**, with one sign of voltage applied to the cell. Field reversal then produces a reorientation of $\sim 2\theta$ of **n**, giving clear absorption changes. Figure 4 shows such data taken in the Sm-C* phase at T = 70 °C, where $\theta = 28.9°$. The transient reorientation and its saturation is evident in the four distinct vibrational modes studied. The change in absorbance observed can be qualitatively understood for each mode in terms of β, the angle between its absorption dipole and the molecular long axis; The *phenyl* core vibration has $\beta \sim 0°$, and thus the largest change in absorbance, the *alkyl* CH_2 stretching vibration has $\beta \sim 90°$, for an all-trans tail, with the change in absorbance being reduced because of disorder in the tails; The *nitro* stretching vibration has $\beta \sim 30°$; and the *carbonyl* stretching vibration has $\beta \sim 60°$ and shows a small change in absorbance because this β is close to the "magic angle", $\beta \sim 54.7°$, for which a uniaxial distribution about the long axis appears isotropic.

For full data collection time-resolved peak absorbance for each vibration is obtained by fits to the spectra for a series of Ω, spaced by 10° intervals.

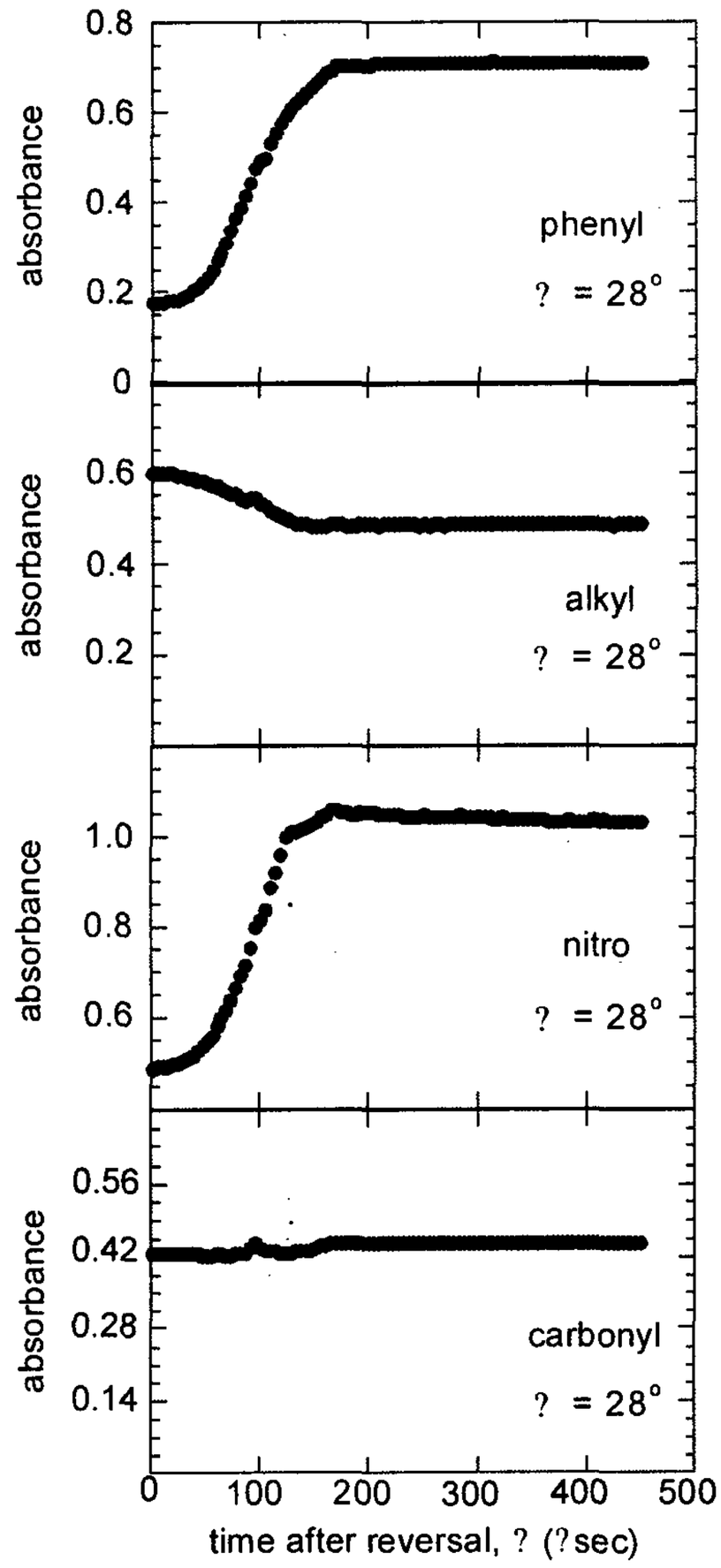

Figure 4. Absorbance changes upon field reversal for the phenyl, alkyl, NO_2, and C=O group modes at T=70 °C.

The results are displayed in Figure 5 as polar plots of peak absorbance $A(\Omega)$, which effectively exhibit the dichroism of each mode, and its evolution with time. Ignoring birefringence, $A(\Omega)$ for any mode must be of the form (1) where the absorbances A_{para} (A_{perp}) are those measured with IR polarizer parallel (perpendicular) to the $\Omega=\Omega_o$ axis, the polarizer orientation for either maximum (A_{max}) or minimum (A_{min}) absorbance.

$$A(\Omega) = -\log\{(10^{-A_{max}})\cos^2(\Omega - \Omega_o) + (10^{-A_{min}})\sin^2(\Omega - \Omega_o)\}. \quad (1)$$

Polar plots of A(Ω) for the *phenyl*, *alkyl* and *nitro* modes for time after field reversal τ = 0, 75,

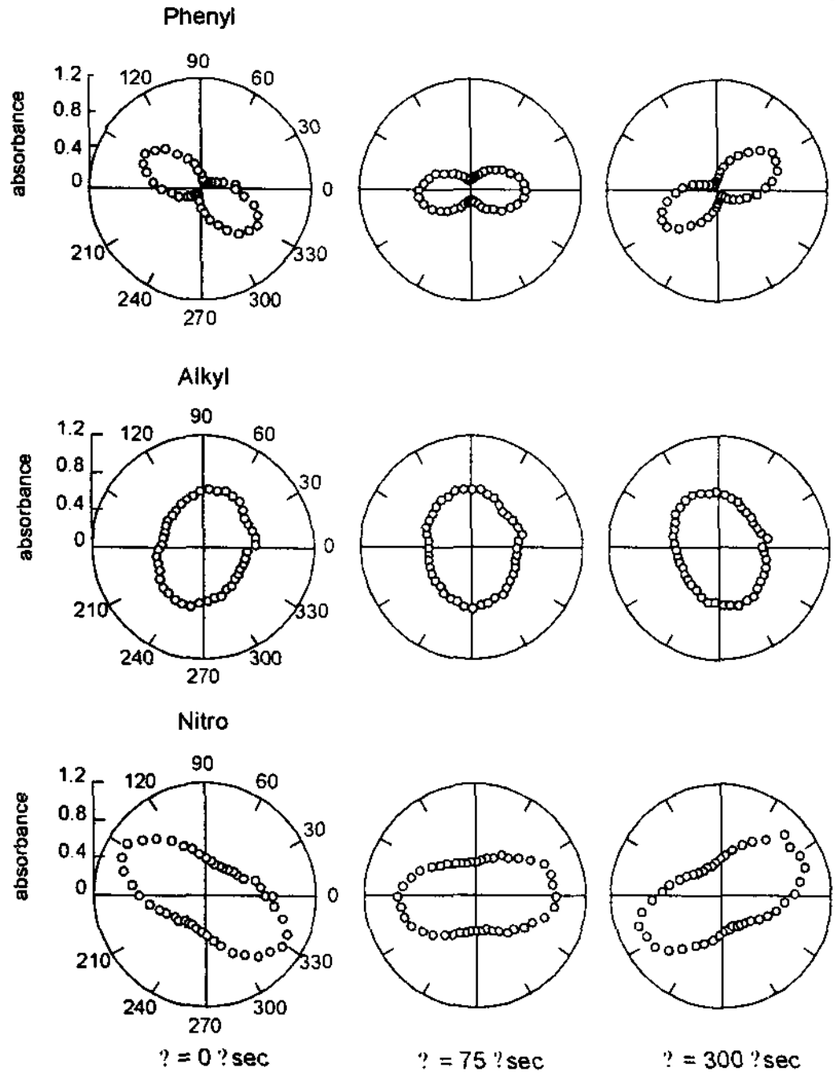

Figure 5. Polar plots of IR absorbance vs. IR polarizer orientation Ω for (a) 0 μs (b) 75 μs and (c) 300 μs time delay following field reversal at T=70 °C.

and 300 μs are shown in Figure 5. The reorientation of Ω_o with field reversal is evident.

3. Results and Discussion

Fitting of Eq. (1) to A(Ω) enables the determination of Ω_o vs. τ, with the result shown in Fig. 6(a) for the *phenyl* and *nitro* (core) and *alkyl* (tail) vibrations, Ω_o giving the IR polarizer orientation of A_{max} (A_{min}) for the *phenyl* and *nitro* (*alkyl*) vibrations. As can be seen, while the dynamics of the core and tail appear to be similar, there is a marked difference between the asymptotic $\Omega_o\ (T)_{phenyl} \equiv \Omega_o\ (T, \tau\rightarrow\infty)_{phenyl}$, and $\Omega_o\ (T)_{alkyl} \equiv \Omega_o\ (T, \tau\rightarrow\infty)_{alkyl}$, with the net reorientation of the phenyl vibration considerably larger than that of the other modes. Fig 6(b) shows the time dependence of $\Delta\Omega_o\ (T, \tau) \equiv \Omega_0(T, \tau)_{phenyl} - \Omega_0(T, \tau)_{alkyl}$, the difference in Ω_0 for the phenyl and alkyl vibrations at T=70 °C, which has a time dependence similar to that of $\Omega_0(T, \tau)_{phenyl}$ and $\Omega_0(T, \tau)_{alkyl}$ themselves. The time dependence of $\Omega_0(T)_{phenyl} - \Omega_0(T)_{alkyl}$, the difference in Ω_0 for the *phenyl* and *alkyl* vibration at T =70 °C, which has a time dependence similar to that of $\Omega_0(T, \tau)_{phenyl}$, and $\Omega_0(T, \tau)_{alkyl}$ and themselves. The asymptotic values of $\Omega_0(T)_{phenyl}$ and $\Omega_0(T)_{alkyl}$ and their difference are consistent with the results from static dichroism measurements, shown in Fig 7.

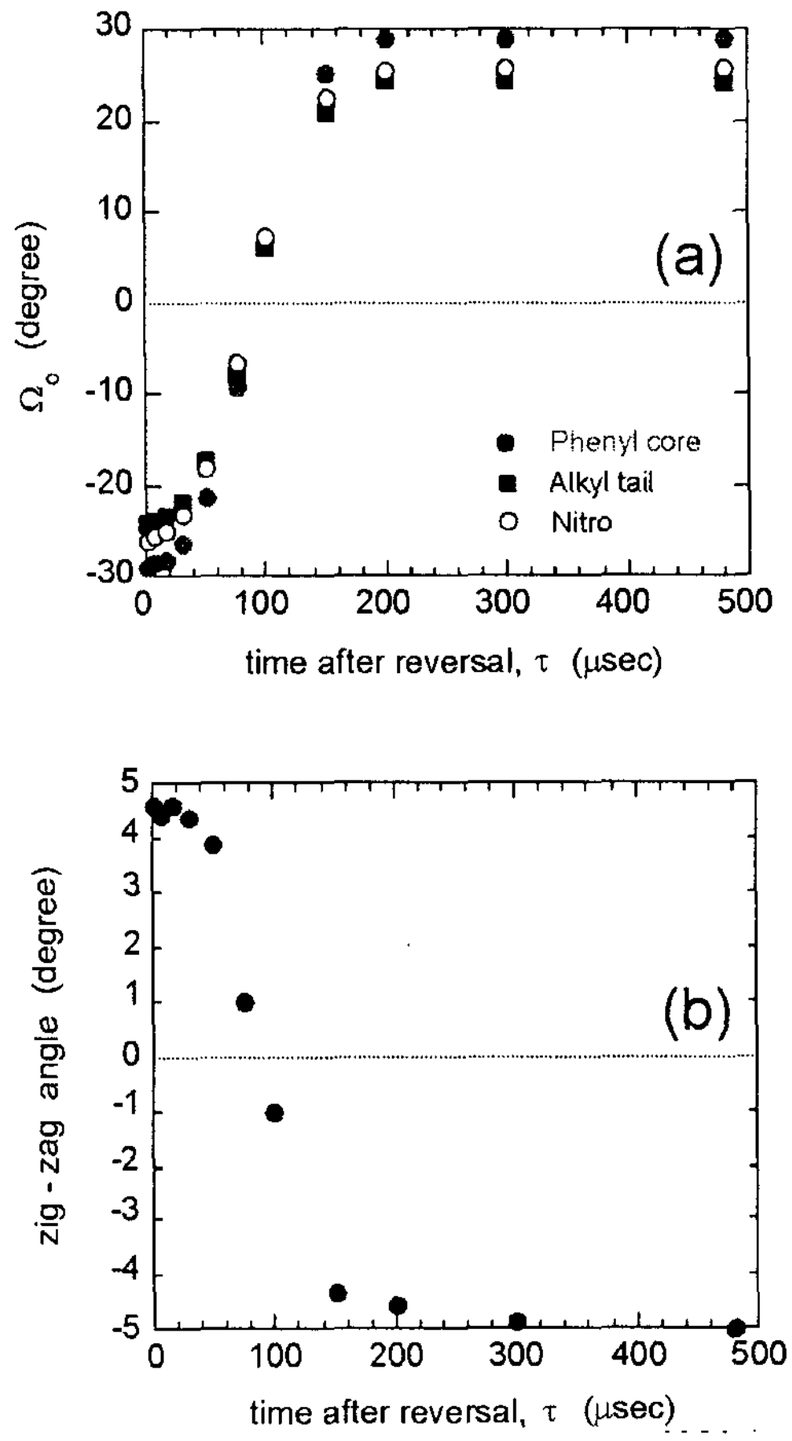

Figure 6. (a) Time dependence following field reversal of $\Omega_0(\tau)$, the IR polarizer orientation of A_{max} (A_{min}) for the phenyl and nitro (alkyl) vibrations. (b) Time dependence of the "zig-zag" angle $\Delta\Omega_o\ (T, \tau) \approx \Omega_0(T, \tau)_{phenyl} - \Omega_0(T, \tau)_{alkyl}$

Here we plot the visible light optic axis tilt relative to the layer normal θ(T), along with $\Omega_0(T)_{phenyl}$ and $\Omega_0(T)_{alkyl}$ and their difference $\Delta\Omega_o\ (T, \tau) \equiv \Omega_0(T, \tau)_{phenyl} - \Omega_0(T, \tau)_{alkyl}$. The dynamic IR measurements reported here have

been carried out at T=70 °C and 40 °C, at which $\Delta\Omega_o$ (T)~6° and 9°, respectively.

The three parameters A_{max}, A_{min}, and Ω_0 are related to $\langle p_i p_j \rangle_m$ the moments of the orientation distribution of the mode absorption dipole **p**, which is proportional to the imaginary part of the contribution of the mode to the dielectric tensor $(\delta\varepsilon_{ij})_m \propto \langle p_i p_j \rangle_m$. The Ω_0 axis is the projection, onto the **y-z** plane of polarization of the IR light, of a principle axis of $\langle p_i p_j \rangle_m$ or $(\delta\varepsilon_{ij})_m$. In the static Sm-C or Sm-C* phase, the coordinate system which diagonalizes the matrix $\langle p_i p_j \rangle$ has one axis parallel to the twofold rotation axis, i.e., parallel to the polarization $\mathbf{P}_s$ in the Sm-C* phase, and has the other two axes in the Sm-C tilt plane, normal to $\mathbf{P}_s$. Thus with the field applied in the geometry of Fig 1, $\langle p_x p_z \rangle = \langle p_x p_y \rangle = 0$, and A(Ω) is determined by the three moments, $\langle p_y^2 \rangle$, $\langle p_z^2 \rangle$, and $\langle p_y p_z \rangle$, of the orientation distribution.

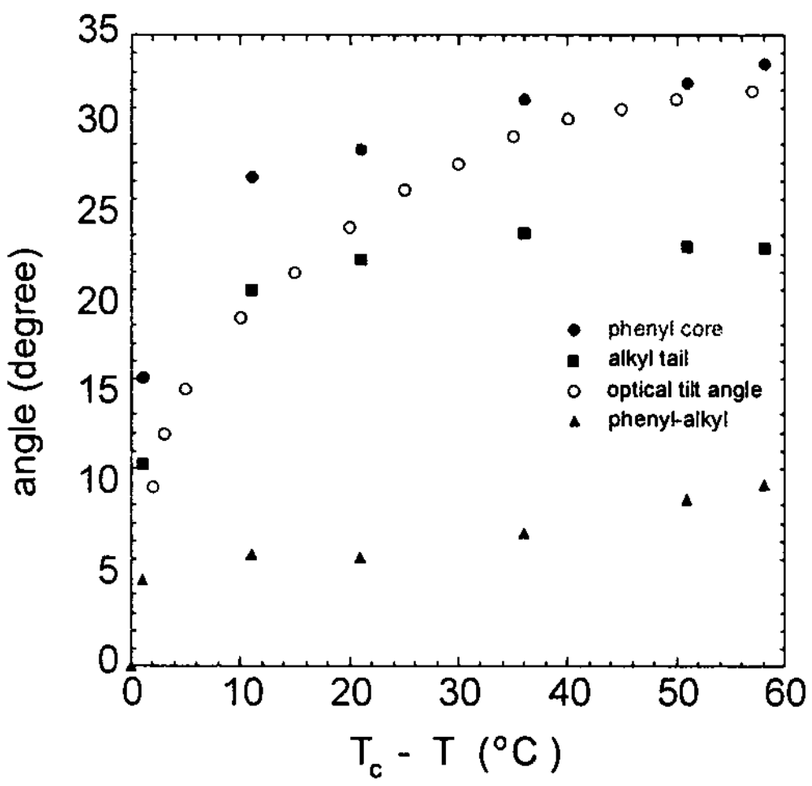

Since the transition dipole for the *phenyl* transition is parallel to the core, the coordinate system diagonalizing $\langle p_i p_j \rangle_{phenyl}$ has an axis parallel to the core, and $\Omega_0(T)_{phenyl}$ is a measure of the mean core orientation projected onto the tilt plane. Thus, the finite $\Delta\Omega_0$ indicates that the molecular orientation in the phase has the tails less tilted on average than the cores, by the angle $\Delta\Omega_0$ which approaches 10° in Sm-C* at low T, and thus than the mean molecular configuration is bent. Since $\Omega_0(T)_{phenyl}$ is a good measure of the actual core tilt, it is comparable to the optic axis tilt, which is determined largely by the optical anisotropy of the core, with a principal axis also at nearly $\Omega_0(T)_{phenyl}$. The optic axis orientation is, in Fig 7, slightly smaller than $\Omega_0(T)_{phenyl}$, possibly because of the contribution of the tails to the birefringence. This larger tilt of the cores relative to the tails is a generic feature of the Sm-C phase, as measured by x-ray diffraction, than expected on the basis of the optic axis tilt[7], determined primarily by the core.

Given the Sm-C two fold axes, parallel to **x** in the layer midplanes, the mean molecular organization with the tails less tilted than the cores implies that the molecular mean field or binding site imposed on a molecule by its neighbors is zig-zag-shaped (a zig-zag bent cylindrical hole), and leads to a natural explanation of the polar ordering about the molecular long axis in the Sm-C phase, since, in general, only a single orientation of a bent molecular conformation about its long axis will minimize energy in a zig-zag shaped binding site [8].

4. Conclusion

We confirm, using time-resolved IR spectroscopy, that the response of Sm-C* W314 to field reversal is polarization reversal via field-induced rotation of the molecular director around on the Sm-C* tilt cone. During this rotation the dynamics of the molecular core and tail segments is identical in the sense that the average molecular conformation appears to rotate on the cone as a rigid unit, with both tail and core transition moment axes confined to the same (rotating) tilt plane (passing through the layer normal projection at the same time) and keeping a fixed relative tilt (zig-zag) angle.

5. References

[1] W. G. Jang, C. S. Park, J. E. Maclennan, K. H. Kim, and N. A. Clark, Ferroelectrics **180**, 213 (1996).

[2] K. H. Kim, K. Ishikawa, H. Takezoe, and A. Fukuda, Phys. Rev. E **51**, 2166 (1995).

[3] W. Uhman, A. Becker, C. Taran, and F. Siebert, Appl. Spectroscopy, **45**, 390 (1991).
[4] K. Matsutani, H. Sugisawa, A. Yokota, Y. Furukawa, and M. Tatsumi, Appl. Spectroscopy , **46**, 560 (1992).
[5] R. B. Meyer, L. Liebert, L. Strzelecki, and P. Keller, J. Phys. (France) **36**, L-69 (1975).
[6] N. A. Clark and S. T. Lagerwall, Appl. Phys. Lett. **36**, 899 (1980).
[7] T. P. Rieker, N. A. Clark, G. S. Smith, D. S. Parmar, E. B. Sirota, and C. R. Safinya, Phs. Rev. Lett. **59**, 2658 (1987)
[8] D. M. Walba and N. A. Clark, Ferroelectrics **84**, 65 (1988).